Cement & Concrete Composites 36 (2013) 85–92

Contents lists available at SciVerse ScienceDirect

Cement & Concrete Composites

journal homepage: www.elsevier.com/locate/cemconcomp

Micromechanical analysis of heterogeneous structural materials

Jiří Němeček *, Vlastimil Králík, Jaroslav Vondřejc

Czech Technical University in Prague, Department of Mechanics, Faculty of Civil Engineering, Thákurova 7, 166 29 Prague 6, Czech Republic

ARTICLE INFO

Article history:
Received 31 January 2012
Received in revised form 25 June 2012
Accepted 26 June 2012
Available online 5 July 2012

Keywords:
Micromechanics
Nanoindentation
Heterogeneous materials
Grid indentation
Deconvolution
Homogenization
FFT

ABSTRACT

This paper shows an efficient methodology based on micromechanical framework and grid nanoindentation for the assessment of effective elastic properties on several types of microscopically heterogeneous structural materials. Such task is a prerequisite for successful nano- and micro-structural material characterization, development and optimization. The grid nanoindentation and statistical deconvolution methods previously described in the literature e.g. for cementitious materials [1,2], alkali activated materials [3] or high-performance concretes [4] have been employed. In this paper we demonstrate their utilization also for other types of structural composites with crystalline nature and we validate the results by using enhanced numerical method based on fast Fourier transform (FFT). The direct procedure of using grid nanoindentation data in the FFT method simplifies the evaluation of effective composite properties and leads to the assemblage of the full stiffness matrix compared to simple analytical approaches.

The paper deals namely with cement paste, gypsum and aluminum alloy. Nanoindentation is used for the determination of phase properties in grid points at the scale below one micrometer. Statistical approach and deconvolution methods are applied to assess intrinsic phase properties. Elastic properties obtained by nanoindentation are homogenized in the frame of the representative volume element (RVE) by means of analytical and numerical FFT-based schemes. Good correlation of the results from all methods was found for the tested materials due to the close-to-isotropic nature of the composites in the RVE having dimensions ~100–200 μm. Results were also verified against macroscopic experimental results. The proposed and validated numerical approach can be successively used for the material modeling in finite element software or for optimization of materials with inhomogeneous microstructures.

1. Introduction

Structural composites such as concrete, gypsum, metals and others are often characterized by a heterogeneous microstructure at different length scales (nm to m). Traditionally, their mechanical properties are assessed from macroscopic tests on samples with cm to m dimensions that can only describe overall (averaged) properties like overall Young's modulus or strength. Nowadays, nanoindentation [5] can be successfully applied to access the nanometer scale and to assess individual phase properties like C–S–H gels, Portlandite or clinker. However, the properties extracted from nanoindentation are measured for small material volumes (nm to μm). The large gap between the scales can be crossed by using multiscale models and micromechanical framework which uses the concept of the representative volume element (RVE) [6] defined for each material level. Homogenization of individual contributions of the RVE microstructural components is provided by multiple micromechanical approaches that search for effective properties by solving matrix-inclusion problems. There is a variety of analytical methods and estimates (Voigt, Reuss or Hashin–Strikmann bounds, Mori–Tanaka method, self-consistent scheme and others [6]) that usually need to assess phase properties and their volume fractions prior to the analysis. Such assessment is not straightforward in the case of structural composites whose microstructure develops in space and time during their lifetime. Therefore, statistical estimates obtained from grid nanoindentation need to be employed. The grid nanoindentation and statistical deconvolution methods have been described and used e.g. by Ulm and coworkers [1,2] for cement based materials, Němeček et al. [3] for alkali activated materials or Sorelli et al. [4] for high performance concrete.

In the case of numerical methods (e.g. finite elements or FFT based methods), homogenization can be much easier due to the direct use of grid point mechanical data as will be demonstrated later in the paper.

2. Methods

In this paper, we first deal with the evaluation of nanoindentation data received from large statistical sets (hundreds of indents) on the scale of several hundreds of micrometers which is a scale

* Corresponding author. Tel.: +420 224 354 309.
E-mail addresses: jiri.nemecek@fsv.cvut.cz (J. Němeček), vlastimil.kralik@fsv.cvut.cz (V. Králík), jaroslav.vondrejc@fsv.cvut.cz (J. Vondřejc).

0958-9465/$ - see front matter © 2012 Elsevier Ltd. All rights reserved.
http://dx.doi.org/10.1016/j.cemconcomp.2012.06.015

that includes all material phases within RVE in a sufficient content. Since the microstructure of the composites is very complex in this scale and the determination of pure individual micromechanically distinct phases is not straightforward, we assess the individual properties by using grid indentation technique [2] with subsequent statistical deconvolution method [2–4]. Mathematically, the deconvolution is an ill-posed problem that can be regularized by a prior setting of the number of mechanically different phases that are determined. Therefore, we link this number with the number of chemically different phases or groups of mechanically similar constituents as described in Section 6. We also adapt the originally proposed deconvolution method [2] by using different minimizing criteria and modified Monte Carlo simulations as described in Němeček et al. [3]. Such methodology gives us mean phase properties together with the estimation of their volume fractions based on the experimental dataset from the whole grid.

After setting the RVE size and receiving phase properties, effective elastic properties are determined by both analytical and numerical homogenization schemes. The comparison of the methods is provided by comparing the differences between the output stiffness matrices. As mentioned earlier, the application of the numerical scheme does not require the knowledge of intrinsic phase properties and the direct use of grid data is utilized.

3. Tested materials and test setup

3.1. Cement paste

Selected heterogeneous structural materials were chosen for this study. At first, cement paste samples were prepared from Portland cement CEM-I 42,5 R (locality Mokrá, CZ) with water to cement weight ratio equal to 0.5 [7]. Samples were stored in water for two years. Therefore, high degree of hydration (over 90%) can be anticipated in the samples. The microstructure of cement paste in the tested volume includes several chemical phases known from cement chemistry, namely low- and high- density calcium–silica hydrates (LD and HD C–S–H), calcium hydroxide $Ca(OH)_2$, residual clinker, porosity and some other minor phases. The cement paste microstructure is shown in Fig. 1a. Very light areas in Fig. 1a can be attributed to the residual clinker, light grey areas are rich of $Ca(OH)_2$, dark grey zone belongs to C–S–H gels and black color represents very low density regions or capillary porosity. Note, that C–S–H gel and $Ca(OH)_2$ zones are spatially intermixed in small volumes (<<10 μm) and the resolution of SEM–BSE images does not allow for a direct separation of these phases from the image. The majority of the material volume mostly consists of poorly crystalline or amorphous phases (C–S–H) and partly of crystalline phases ($Ca(OH)_2$). Portlandite crystals are known for their anisotropy. Since their size and volume is not large in the sample and they can be mixed with C–S–H, all phases will be supposed to be mechanically isotropic for simplification in the analysis.

Cement paste includes also wide distribution of pores. Majority of pores lies in the nanometer range (<100 nm, as checked with He/Hg-porosimetry) and, on the other hand, large capillary pores are present in the scale above the indentation level (i.e. >>1 μm). Therefore, the indentation depth was chosen so that the nanoporosity was included in the tested volume but the large capillary porosity was not. The depth range ~100–300 nm was suitable for the analysis.

Cement paste was indented by a grid consisting of $20 \times 20 = 400$ indents with 10 μm spacing which yields the RVE size ~200 μm. The indents were prescribed as load controlled (maximum force 2 mN, loading/unloading rate 12 mN/min, holding for 30 s). Examples of load-penetration diagrams for different constituents are shown in Fig. 2a. The final penetration depths vary for the phases depending on their stiffness.

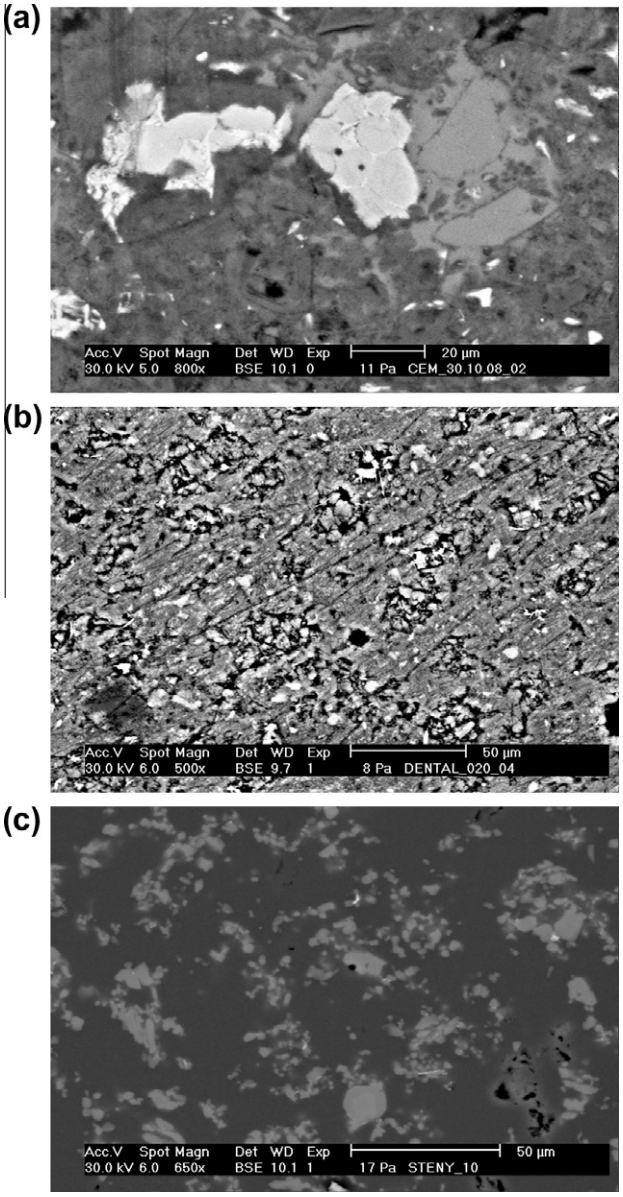

Fig. 1. Microstructures of (a) cement paste, (b) gypsum and (c) Al-alloy.

3.2. Gypsum

Secondly, dental gypsum (Interdent®) was chosen as a model representative for gypsum based materials. Samples were prepared with water to gypsum ratio 0.2 and matured in ambient conditions for two months. From the chemistry point of view, every gypsum binder is composed of three main components – calcium sulfate anhydrite ($CaSO_4$), calcium sulfate hemihydrate ($CaSO_4{\cdot}½H_2O$) in two modifications: α- or β-hemihydrate, and calcium sulfate dihydrate ($CaSO_4{\cdot}2H_2O$). The gypsum binder includes also some impurities and additives in the case of natural sources. The Interdent gypsum is a low-porosity purified α-hemihydrate used for dental purposes.

The hardened gypsum mass is a porous material with a relatively large internal surface consisting of interlocking crystals in the form of plates and needles (Singh and Middendorf [8]). Note

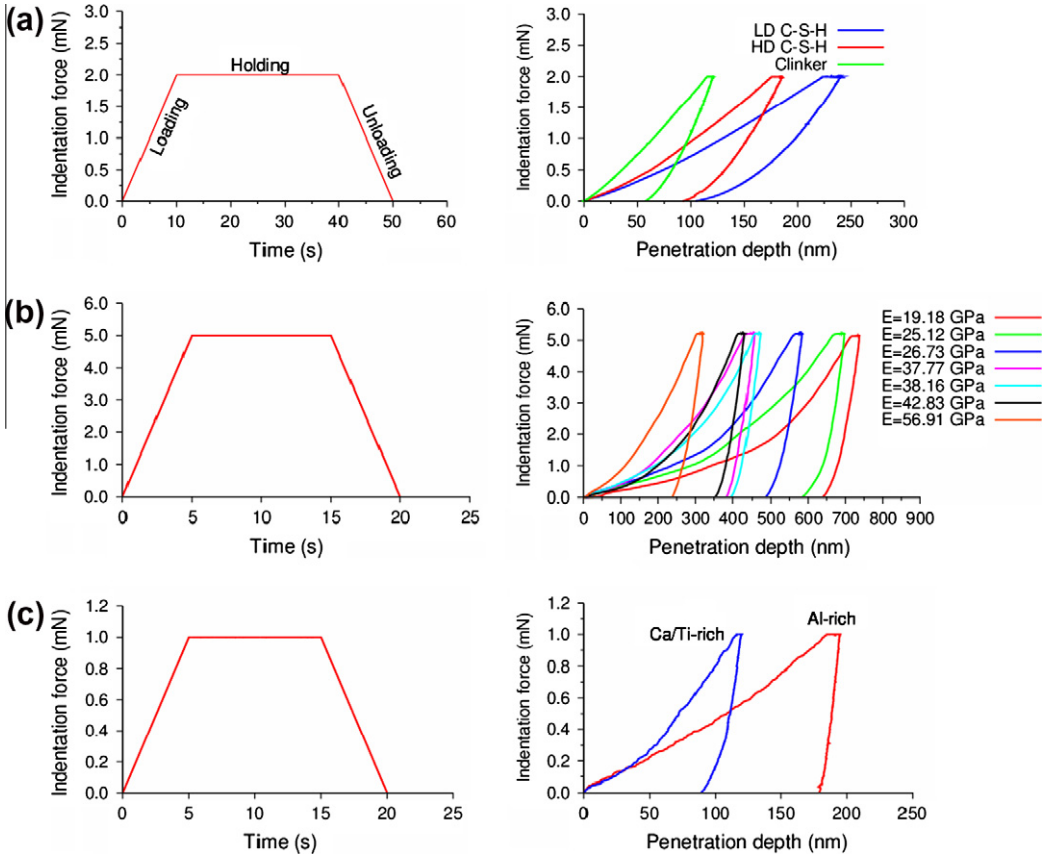

Fig. 2. Nanoindentation load–time and load–depth diagrams for (a) cement paste, (b) gypsum and (c) Al-alloy.

that in the case of β-hemihydrate hydration, the resulting sample porosity is typically very large (more than 50% for higher water to binder ratii) and crystals are interlocked very weakly. Therefore, ordinary gypsum systems used for building purposes which are based on β-hemihydrate are characterized with relatively low strengths (<10 MPa in compression). In contrast, hydration of our samples based on α-hemihydrate produced a dense matrix with total sample porosity just 19%. The majority of pores lay in the nano-range 0–300 nm (0–100 nm 7%, 100–300 nm 4%, 300–1000 nm 1%) and virtually no pores appeared between 1 and 100 μm (<0.5%). Due to the very low porosity, the strength of this material is much higher (>50 MPa in compression). The gypsum microstructure is depicted in Fig. 1b in which dark areas can be attributed to the porosity, very light areas belong to low hydrated $CaSO_4$ grains or carbonates. The majority of the sample volume in Fig. 1b composes of hydrated crystalline mass.

Two locations were tested on gypsum samples. Each place was covered by $15 \times 12 = 180$ indents with 15 μm spacing. Similar loading as in the case of cement was used (load controlled test to maximum force 5 mN). Typical loading diagrams are depicted in Fig. 2b. A bit wider range of final depths on indented phases (200–800 nm) was obtained due to larger differences in the phase stiffness. However, the majority of indents were performed to the mean final depths around 400–500 nm. The RVE size defined by the tested area is again ~200 μm in this case.

3.3. Aluminum alloy

For the sake of comparison with different kind of material, an aluminum alloy used for the production of lightweight aluminum foams Alporas® was also studied [9,10]. The material is produced from an aluminum intermixed with 1.5 wt.% of Ca and 1.6 wt.% TiH_2. Ca/Ti-rich discrete precipitates and diffuse Al_4Ca areas develop in the metal solid [11] that can be seen as lighter areas in Fig. 1c. Therefore, two distinct phases denoted as Al-rich and Ca/Ti-rich were separated in this study.

Nanoindentation was applied to the cell walls of the foam. Loading to maximum force 1 mN was used. Final depths arrived at ~100–200 nm. Typical differences between the loading diagrams of different phases obtained from nanoindentation are shown in Fig. 2c. Results from 200 indents (two locations 10×10 indents) with 10 μm spacing were evaluated. The RVE size related to the tested region is ~100 μm in this case.

4. Nanoindentation, sample preparation and evaluation of phase properties

As mentioned above, nanoindentation has been applied to receive elastic constants of individual material phases. Nanoindenter (Nanohardness tester, CSM Instruments) located in Prague's laboratory at the Czech Technical University was employed in our measurements. The apparatus was equipped with a diamond pyramidal Berkovich tip with the apex radius ~100 nm.

The already well-known principle of nanoindentation lies in bringing a very small tip (Berkovich in our case) to the surface of the material to make an imprint. Material constants are deduced from the measured load–displacement curves performed on flat surfaces.

For our measurements, the depth of penetration was kept around ~300 nm for cement paste, ~500 nm for gypsum and ~200 nm for aluminum in order to capture each material phase on one hand and to minimize phase interactions on the other hand. The depth of the affected volume under the indenter tip can be estimated as 3× the penetration depth [2], i.e. around 0.6^3–

1.5^3 μm^3 for the studied cases. Such size roughly corresponds to 1/10 of most of the grains or single phase areas which justifies the use of phase devonvolution [1,2]. The indentation volume contains also a part of nanoporosity that is naturally included in phase results.

All samples were mechanically polished prior to the testing in order to achieve smooth and flat surface with substantially smaller roughness compared to indentation depths. The surface roughness (evaluated as root-mean-square on the scanned area of 10×10 μm) was checked with AFM. It was found to be ~25 nm on cement paste, ~38 nm on gypsum and ~12 nm on Al-alloy. Therefore, the sample roughness was acceptable in relation to the awaited indentation depths.

The indentation loading history contained three segments: loading, holding and unloading periods. The holding period was included in order to minimize creep effects on the elastic unloading [7]. Elastic properties were evaluated for individual indents using analytical formulae derived by Oliver and Pharr [12], which account for an elasto-plastic contact of a conical indenter with an isotropic half-space. The reduced (combined) elastic modulus is then defined as:

$$E_r = \frac{1}{2\beta}\frac{\sqrt{\pi}}{\sqrt{A}}\frac{dP}{dh} \tag{1}$$

in which A is the projected contact area of the indenter at the peak load, β is geometrical constant (β = 1.034 for the used Berkovich tip) and dP/dh is a slope of the unloading branch evaluated at the peak. Elastic modulus E of the measured sample can be found using contact mechanics which accounts for the effect of non-rigid indenter as:

$$\frac{1}{E_r} = \frac{(1-\nu^2)}{E} + \frac{(1-\nu_i^2)}{E_i} \tag{2}$$

in which ν is the Poisson's ratio of the tested material, E_i a ν_i are known elastic modulus and Poisson's ratio of the indenter.

The solution of the contact problem for anisotropic materials can be found in [13,14]. In this work, all material phases were treated as elastically isotropic. Such simplification was adopted due to the following reasons. In cement paste, the degree of crystallinity is poor in the majority of specimen volume (e.g. in C–S–H gel). The content of crystalline $Ca(OH)_2$ phases is low and due to the limited space for the crystal growth the degree of crystallinity decreases.

On the other hand, gypsum is composed of a polycrystalline matter with locally anisotropic character. However, the response in grid nanoindentation is measured on differently oriented crystals and also on a combination of differently oriented crystals located under the indenter in the affected volume ~1.5^3 μm^3. The tested location can be viewed as a set of mechanically different phases that are physically averaged by an indenter. Apparent isotropic elasticity constants associated with the tested indentation volume can be derived in this case. Similarly, isotropic estimates were derived for the measured volume in case of Al-alloy disregarding the local anisotropy on a crystalline level.

The distinction of the chemically and/or mechanically different material phases is often not possible on the microlevel (<1 μm) even with the use of SEM–EDX images. In order to receive statistically relevant data from all material phases, we applied grid indentation over the tested RVE (Fig. 1). Large matrices containing hundreds of indents have been performed on tested samples (see Section 3). To assess individual phase properties, statistical deconvolution was employed [2,3]. In this method, experimental data are analyzed from the frequency plots. Mean elastic properties as well as phase volume fraction are estimated based on the best fit of the experimental data with a limited number of Gauss distributions (Fig. 3).

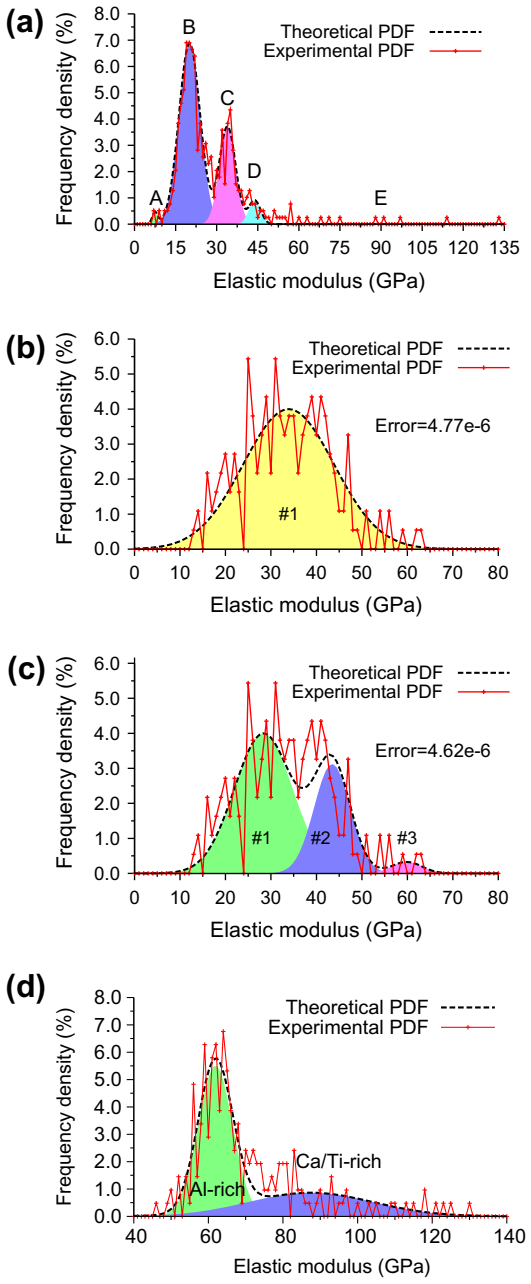

Fig. 3. Deconvolution of modulus of elasticity frequency plots into mechanical phases on (a) cement paste, (b) gypsum three phases fit (c) gypsum single phase fit and (d) Al-alloy.

5. Micromechanical homogenization

5.1. Analytical and numerical schemes

In general, homogenization methods search for effective material properties. The previously mentioned concept of RVE which includes all microstructural inhomogeneities that should be substantially smaller than the RVE size is utilized. The homogenization problem can be solved either by analytical methods or by numerical approximations. Analytical schemes often rely on simplified assumptions concerning inclusion geometry, boundary conditions or isotropy. More complex results can be obtained from numerical methods that are based on finite element solution or fast Fourier transformation (Moulinec and Suquet [17]), for instance.

The classical analytical solution based on constant stress/strain fields in individual microscale components for an ellipsoidal inclusion embedded in an infinite body was derived by Eshelby [15]. Effective elastic properties are then obtained through averaging over the local contributions. Various estimates considering different geometrical constraints or special choices of the reference medium such as the Mori–Tanaka method or the self-consistent scheme [6,16] can be used. For the case of a composite material with prevailing matrix and spherical inclusions the Mori–Tanaka method [16] was previously found to be a simple but powerful tool to estimate effective composite properties also for structural materials [2] and, therefore, it was used in this work. In the Mori–Tanaka method, the homogenized isotropic bulk and shear moduli of an r-phase composite are assessed as follows:

$$k_{\text{hom}} = \frac{\sum_r f_r k_r \left(1 + \alpha_0 \left(\frac{k_r}{k_0} - 1\right)\right)^{-1}}{\sum_r f_r \left(1 + \alpha_0 \left(\frac{k_r}{k_0} - 1\right)\right)^{-1}} \tag{3}$$

$$\mu_{\text{hom}} = \frac{\sum_r f_r \mu_r \left(1 + \beta_0 \left(\frac{\mu_r}{\mu_0} - 1\right)\right)^{-1}}{\sum_r f_r \left(1 + \beta_0 \left(\frac{\mu_r}{\mu_0} - 1\right)\right)^{-1}} \tag{4}$$

$$\alpha_0 = \frac{3k_0}{3k_0 + 4\mu_0}, \quad \beta_0 = \frac{6k_0 + 12\mu_0}{15k_0 + 20\mu_0} \tag{5}$$

where the subscript 0 corresponds to the reference medium and r corresponds to a particulate inclusion. Thus, k_0 and μ_0 are the bulk and shear moduli of the reference medium, while k_r and μ_r refer to the inclusion phases. Further, bulk and shear moduli can be recomputed to engineering values of elastic modulus and Poisson's ratio as:

$$E = \frac{9k\mu}{3k + \mu}, \quad \nu = \frac{3k - 2\mu}{6k + 2\mu} \tag{6}$$

Materials with no preference of matrix phase (e.g. polycrystalline metals) are usually modeled with the self-consistent scheme [6]. It is an implicit scheme, similar to the Mori–Tanaka method, in which the reference medium points back to the homogenized medium itself.

Local strain and stress fields in a RVE can also be found by numerical methods like finite element method or a method based on fast Fourier transformation (FFT). The later one was proven to be a reliable and computationally inexpensive method which only utilizes mechanical data in the regular grid (i.e. equidistant discretization points). Such a concept perfectly matches with the concept of the grid nanoindentation. Therefore, the FFT method was chosen for our purposes. The numerical scheme used here solves the problem of finding the effective elasticity tensor with a periodically repeating RVE by using discretization of an integral Lippmann–Schwinger equation:

$$\varepsilon(\mathbf{x}) = \varepsilon^0 - \int_\Omega \Gamma^0(\mathbf{x} - \mathbf{y}) : (L(\mathbf{y}) - L^0) : \varepsilon(\mathbf{y}) d\mathbf{y} \tag{7}$$

in which ε and L stand for the local strain and stiffness tensor, respectively, and ε^0 is the homogenized strain defined as a spatial average over RVE domain Ω as

$$\varepsilon^0 = \langle \varepsilon \rangle = \frac{1}{\Omega} \int_\Omega \varepsilon(\mathbf{x}) d\mathbf{x} \tag{8}$$

Γ^0 is the periodic Green operator associated with the reference elasticity tensor L^0 which is a parameter of the method [17,18]. The problem is further discretized using trigonometric collocation method [19,20] which leads to the assemblage of a nonsymmetrical linear system of equations:

$$[I + F^{-1} \hat{\Gamma} F (L - L^0)] e = e^0 \tag{9}$$

where the vector e stores a strain field at discretization points and e^0 the macroscopic strain, L and L^0 stores the material coefficients at discretization points and reference elasticity tensor respectively, I denotes the identity matrix, $\hat{\Gamma}$ stores the values corresponding to the integral kernel in the Fourier space, and F (F^{-1}) stores the (inverse) discrete Fourier transform matrices that can be provided by fast Fourier transform algorithm. The possibility to solve the nonsymmetric linear system by the conjugate gradient method (CG) is proposed by Zeman et al. in [21], where also the particular expression of individual matrices can be found for the problem of electric conductivity or heat transfer. The linear system (Eq. (9)) depends only on stiffness coefficients at grid points that can be obtained using nanoindentation and thus the homogenized (effective) tensor (further denoted as L_{eff}^{FFT}) can be calculated.

In practice, the homogenization procedure includes several steps:

(1) Definition of a periodic unit cell (PUC) with discretization points corresponding to indents' locations (a regular grid).
(2) Assessment of Young's moduli E and Poisson's ratii ν with the help of nanoindentation in grid points (Oliver and Pharr method [12] was used for the extraction of Young's moduli from load–displacement indentation curves).
(3) Assemblage of local elastic stiffness tensors in grid points (plane strain assumption used) which in Mandel's notation reads:

$$L = \frac{E}{(1+\nu)(1-2\nu)} \begin{bmatrix} 1-\nu & \nu & 0 \\ \nu & 1-\nu & 0 \\ 0 & 0 & 1-2\nu \end{bmatrix} \tag{10}$$

(4) Calculation of local strain (from a linear system, Eq. (9), using CG algorithm [21]) and stress fields ($\sigma = L{:}e$) in grid points when applying homogeneous macroscopic strain (unit loads e^0) to the PUC domain.
(5) Calculation of an average stress in the PUC by integration over its volume

$$\langle \sigma \rangle = \frac{1}{\Omega} \int_\Omega \sigma d\mathbf{x} \tag{11}$$

(6) Calculation of the homogenized elasticity tensor for PUC from average stress and prescribed macroscopic strain

$$L_{eff}^{\text{FFT}} : e^0 = \langle \sigma \rangle \tag{12}$$

The resulting homogenized stiffness matrix for PUC must be symmetric, positive definite, but generally anisotropic. The resulting anisotropy of the matrix depends on the topology of inclusions in PUC regardless of the fact that the individual points are treated as locally isotropic. Note also, that the FFT homogenization takes no assumptions on the morphology of the phases as in the case of analytical schemes. It works only with the stiffness coefficients distributed within the PUC and its accuracy depends only on the density of the grid points.

5.2. Comparison of analytical and numerical schemes

The simple analytical methods used in this work (Mori–Tanaka, self-consistent) operate with the assumption of isotropic effective properties. Such assumption is usually acceptable for disordered structural materials. In this case, the isotropic stiffness matrix and plane strain conditions takes the form (in Mandel's notation):

$$L^A_{eff} = \frac{E_{eff}}{(1+\nu_{eff})(1-2\nu_{eff})}\begin{bmatrix} 1-\nu_{eff} & \nu & 0 \\ \nu & 1-\nu_{eff} & 0 \\ 0 & 0 & 1-2\nu_{eff} \end{bmatrix} = \begin{bmatrix} k+\frac{4}{3}\mu & k-\frac{2}{3}\mu & 0 \\ k-\frac{2}{3}\mu & k+\frac{4}{3}\mu & 0 \\ 0 & 0 & 2\mu \end{bmatrix} \quad (13)$$

in which E_{eff} and ν_{eff} are analytically computed effective Young's modulus and Poisson's ratio, respectively. Alternatively, effective bulk and shear moduli k and μ can be used for the calculation. The difference between this stiffness matrix and that received from FFT homogenization can be expressed using a stiffness error norm:

$$\delta = \sqrt{\frac{\left(L^{FFT}_{eff} - L^A_{eff}\right)::\left(L^{FFT}_{eff} - L^A_{eff}\right)}{\left(L^{FFT}_{eff}::L^{FFT}_{eff}\right)}} \quad (14)$$

in which L^{FFT}_{eff} is the (anisotropic) effective stiffness matrix computed by the FFT method.

To assess the degree of anisotropy of the L^{FFT}_{eff} matrix, one can use different measures. Here, we define the degree of anisotropy as:

$$\delta_{ISO} = inf_{L_{ISO}} \sqrt{\frac{\left(L^{FFT}_{eff} - L_{ISO}\right)::\left(L^{FFT}_{eff} - L_{ISO}\right)}{\left(L^{FFT}_{eff}::L_{ISO}\right)}} \quad (15)$$

where the infimum is taken over all isotropic positive definite matrices. We simply calculate the upper estimate $\delta^{FFT}_{ISO} \geqslant \delta_{ISO}$:

$$\delta^{FFT}_{ISO} = \sqrt{\frac{\left(L^{FFT}_{eff} - L^{FFT}_{ISO}\right)::\left(L^{FFT}_{eff} - L^{FFT}_{ISO}\right)}{\left(L^{FFT}_{eff}::L^{FFT}_{ISO}\right)}} \quad (16)$$

by a particular choice of an isotropic matrix:

$$L^{FFT}_{ISO} = \begin{bmatrix} k_{ISO}+\frac{4}{3}\mu_{ISO} & k_{ISO}-\frac{2}{3}\mu_{ISO} & 0 \\ k_{ISO}-\frac{2}{3}\mu_{ISO} & k_{ISO}+\frac{4}{3}\mu_{ISO} & 0 \\ 0 & 0 & 2\mu_{ISO} \end{bmatrix} \quad (17)$$

with

$$\mu_{ISO} = \frac{L^{FFT}_{eff,33}}{2}, \quad k_{ISO} = \frac{L^{FFT}_{eff,11} + L^{FFT}_{eff,22}}{2} - \frac{4}{3}\mu_{ISO}.$$

6. Results and discussion

The resulting frequency plot of elastic moduli measured on cement paste merged from all positions (400 indents) was deconvoluted into five mechanical phases (that correspond to chemical ones) as specified in Table 1. Note, that the values in Table 1 (and similarly in Tables 2 and 3) were found as the best fit in the minimization problem solved by the deconvolution algorithm. The bin size was set to 1 GPa in the construction of probability density functions (PDFs). Ulm et al. [1] suggested the use of cumulative density function (CDF) in the deconvolution rather than PDF. Using CDF does not require the choice of a bin size. On the other hand, using PDF is more physically intuitive and in the case of large dataset leads to similar results.

The deconvoluted phases on cement paste correspond to the peaks shown in Fig. 3a. They are denoted as *A* = low stiffness phase, *B* = low density C–S–H, C = high density C–S–H, D = $Ca(OH)_2$, *E* = clinker. In this case, the notation of mechanically distinct phases matches well with the cement chemistry. Note, that the stiffest microstructural component, the clinker, is not captured well by nanoindentation since the stiffness contrast with respect to other components is too high [2,7]. However, the content of residual clinker is very low in the case of matured paste and it does not significantly influence the rest of the results. Nevertheless, the proper value of elastic modulus for homogenization was taken from ex situ measurements of clinker [7,22].

Two-step homogenization was used in the case of cement paste. Firstly, homogenized properties for the C–S–H level were obtained from low- and high-density C–S–H phases (RVE ~1 μm). Upper level homogenization for RVE (~200 μm) was performed in the second step in which homogenized C–S–H properties were considered together with the rest of the phases (i.e. low stiffness phase, Portlandite and clinker). Results for cement paste are summarized in Table 1. Very similar estimates have been obtained with the Mori–Tanaka and the self-consistent schemes.

Nanoindentation data received on gypsum samples (two locations with 180 indents each) revealed the polycrystalline nature of the composite with an anisotropic character. Since the gypsum crystals are dispersed in the sample volume in a random manner, surface measurements by nanoindentation show high scatter. As mentioned earlier, apparent isotropic moduli associated with the indentation volume ~1.5^3 μm^3 were assessed. The scatter in received results (Fig. 3b) can be treated as a set of mechanically different responses from different crystal orientations. As such, we

Table 1
Data received from statistical deconvolution and homogenized values on cement paste.

Deconvoluted phase	*E* (GPa)	Poisson's ratio	Volume fraction
Low stiffness phase (A)	7.45	0.2	0.011
Low density C–S–H (B)	20.09	0.2	0.632
High density C–S–H (C)	33.93	0.2	0.263
Portlandite (D)	43.88	0.3	0.046
Clinker (E)	121.0[a]	0.3	0.048
Homogenization			
C–S–H level (B + C) by M–T	23.36	0.2	
C–S–H level (B + C) by SCS	23.41	0.2	
Cement paste level (B + C) + A + D + E by M–T	25.39	0.207	1.0
Cement paste level (B + C) + A + D + E by SCS	25.44	0.208	1.0

M–T stands for the Mori–Tanaka scheme; SCS stands for the self-consistent scheme.
[a] *Note*: Clinker value was adjusted to 121 GPa according to [7].

Table 2
Data received from statistical deconvolution to the three phases and homogenized values on gypsum.

Deconvoluted phase	*E* (GPa)	Poisson's ratio	Volume fraction
#1	28.36	0.32	0.663
#2	43.46	0.32	0.310
#3	59.89	0.32	0.027
Homogenization method			
M–T	32.96	0.32	1.0
SCS	33.02	0.32	1.0

Note: M–T stands for the Mori–Tanaka scheme; SCS stands for the self-consistent scheme.

Table 3
Data received from statistical deconvolution and homogenized values on Al-alloy.

Deconvoluted phase	*E* (GPa)	Poisson's ratio	Volume fraction
Al-rich zone	61.88	0.35	0.64
Ca/Ti-rich zone	87.40	0.35	0.36
Homogenization method			
M–T	70.09	0.35	1.0
SCS	70.15	0.35	1.0

Note: M–T stands for the Mori–Tanaka scheme, SCS stands for the self-consistent scheme.

can either use deconvolution to separate mechanically significant groups of these orientations (further denoted as phases) or compute apparent elastic moduli of isotropic solid from all responses in an ensemble (i.e. compute average value from all results). Both approaches have been tested.

The physical motivation for identifying the mechanical phases lies in the fact that gypsum crystallizes in the monoclinic system which is characterized with three significant crystallographic orientations. Therefore, derivation of the three significant peaks by deconvolution of frequency plot was tested (Fig. 3b). Numerical results from this deconvolution are summarized in Table 2.

On the other hand, further simplification based on the assessment of only a single apparent isotropic phase is possible. Then, only one Gaussian distribution is assumed in the calculation. Such fit is depicted in Fig. 3c. The mean value derived from the histogram (E = 33.90 GPa) can be interpreted as an effective gypsum Young's modulus valid for the RVE (~100 μm) which includes also intrinsic nanoporosity.

The difference between the two solutions in terms of an error computed as a sum of squared differences between the experimental and theoretical curves in the deconvolution analysis [3] is very small (~3%). Thus, both fits are almost equally good as indicated in Fig. 3b and c. Also, the comparison of the resulting effective Young's moduli computed by the self-consistent scheme or the Mori–Tanaka method in the case of the three phase medium (Table 2) with an apparent Young's modulus in the case of a single phase (E = 33.90 GPa) shows small differences (~2.7%).

Two mechanically distinct phases were found by the statistical deconvolution (from 200 indents) on Al-alloy sample (Fig. 3c and Table 3). According to the SEM–EDX studies, the dominant phase was denoted as Al-rich zone, whereas the lower stiffness phase as Ca/Ti-rich area. The bin size in the frequency plots was set again to 1 GPa in both cases of gypsum and Al-alloy.

Based on the nanoindentation data analytical homogenization were employed for the assessment of effective RVE elastic properties at first (Tables 1–3). Very similar results have been produced by the Mori–Tanaka method or the self-consistent scheme.

At second, the comparison of stiffness matrices (Eq. (13)) derived from analytical results (Mori–Tanaka scheme was considered for cement pastes and Al-alloy; self-consistent scheme for gypsum), and those from FFT homogenization was performed. Results are specified in the following equations 18–20. The stiffness values are given in GPa. Respective error norms are computed in Eq. (21).

$$\text{cement}: L^{A}_{eff} = \begin{bmatrix} 28.44 & 7.43 & 0 \\ 7.43 & 28.44 & 0 \\ 0 & 0 & 21.02 \end{bmatrix}$$

$$L^{\text{FFT}}_{eff} = \begin{bmatrix} 26.177 & 6.778 & 0.068 \\ 6.778 & 26.224 & 0.014 \\ 0.068 & 0.014 & 19.818 \end{bmatrix} \quad (18)$$

$$\text{Gypsum}: 3 \text{ phase fit}: L^{A}_{eff} = \begin{bmatrix} 47.25 & 22.24 & 0 \\ 22.24 & 47.25 & 0 \\ 0 & 0 & 25.02 \end{bmatrix}$$

$$1\text{phase fit}: L^{A}_{eff} = \begin{bmatrix} 48.51 & 22.84 & 0 \\ 22.84 & 48.51 & 0 \\ 0 & 0 & 25.69 \end{bmatrix}$$

$$L^{\text{FFT}}_{eff} = \begin{bmatrix} 45.302 & 21.185 & 0.101 \\ 21.185 & 45.497 & -0.008 \\ 0.101 & -0.008 & 24.396 \end{bmatrix} \quad (19)$$

$$\text{Al-alloy}: L^{A}_{eff} = \begin{bmatrix} 112.479 & 60.566 & 0 \\ 60.566 & 112.479 & 0 \\ 0 & 0 & 51.913 \end{bmatrix}$$

$$L^{\text{FFT}}_{eff} = \begin{bmatrix} 117.130 & 62.741 & -0.163 \\ 62.741 & 117.106 & -0.143 \\ -0.163 & -0.143 & 54.313 \end{bmatrix} \quad (20)$$

$$\text{Errors}: {}^{\text{cement}}\delta = 0.08, {}^{\text{gypsum}}\delta = 0.07, {}^{\text{Al-alloy}}\delta = 0.04 \quad (21)$$

It is clear from the above equations that both simple analytical and advanced FFT-based method give comparable results in our case. The differences given by error norms for cement and gypsum (7–8%) are acceptable and show good agreement of the results received from different methods. The best agreement of the methods was reached on Al-alloy (error 4%) which can be attributed to the fact that both material phases (Al-rich, and Ca/Ti-rich zones) are even more homogeneously dispersed at microscale RVE compared to the phases that appear in cement paste or gypsum.

The upper bound of the degree of anisotropy for the FFT-based stiffness matrices was assessed by an index defined in Eq. (16) with the following results:

$${}^{\text{cement}}\delta_{ISO} = 0.0132, \; {}^{\text{gypsum}}\delta_{ISO} = 0.0043, \; {}^{\text{Al-alloy}}\delta_{ISO} = 0.0016 \quad (22)$$

Low values in Eq. (22) (0.1–1.3%) show the close-to-isotropic nature of the tested materials within the specified RVE. In other words, microstructural inhomogeneities are uniformly dispersed in the RVE and consequently it also justifies the usage of analytical methods producing isotropic effective (homogenized) properties.

It must be emphasized again that although both analytical and numerical methods give similar results, there is a clear advantage of the FFT method which works directly with the grid indentation data compared to analytical Mori–Tanaka method which needs the assessment of phase properties and volume fractions. Moreover, the full stiffness matrix including possible anisotropy is captured by using the FFT method.

Comparison with macroscopic experimental values of elastic moduli for the given materials also shows good agreement with model predictions. Hydrated compound of cement paste was studied e.g. by Němeček [7] (E = 26.4 ± 1.8 GPa), Constantinides and Ulm [23,24] (E = 22.8 ± 0.5 GPa) or Hughes and Trtik [25] (E = 26.5 GPa). The values correspond well with our results (E = 25.4 GPa).

Gypsum elastic properties were studied e.g. by Meille and Garboczi [26,27] who estimated the plane strain values of the Young's modulus (computed as an angular average from anisotropic crystal elastic moduli tensor) as ~45.7 GPa. Such value was also reported for zero crystal porosity by Sanahuja et al. [28]. If one takes into account an intercrystalline porosity 12% (i.e. the gypsum nanoporosity measured for our specific case; see Section 3.2) the Young's modulus drops down to ~34 GPa [28] which is in excellent agreement with our homogenized value (E = 32–33.90 GPa).

Homogenized Al-alloy properties (E = 70.1 GPa) agree very well with experimental values reported e.g. by Jeon et al. [29] or Ashby et al. [30] (E = 70 GPa).

7. Conclusions

Nanoindentation was successfully used for the assessment of elastic parameters of intrinsic material constituents at the scale below one micrometer and effective composite properties were evaluated with analytical Mori–Tanaka, self-consistent and FFT numerical schemes for three typical structural composites with heterogeneous microstructure. Based on the micromechanical approaches and proposed methodologies we can draw the following conclusions.

(1) It has been shown that the use of grid indentation gives access to both phase properties as well as volume fractions in the case of testing highly heterogeneous microstructures of cement paste, gypsum and Al-alloy.
(2) Effective elastic properties of their microstructural RVEs (100–200 μm) were successfully determined with analytical Mori–Tanaka or self-consistent schemes. However, such approach assumes isotropic nature of the composite with spherical inclusions and several assumptions concerning mainly the number of mechanically different phases and bin size need to be made in the deconvolution algorithm. Therefore, an additional knowledge about the composite microstructure and its microstructural composition is necessary in this case.
(3) Further, numerical FFT-based method was used for the assessment of effective elastic composite properties. The direct use of grid indentation data is employed in this method. The method provides effective stiffness matrix and can capture also possible anisotropy.
(4) The performance of both analytical and numerical approaches was in good agreement for the tested materials mainly due to the close-to-isotropic nature in their RVEs.
(5) Comparison with macroscopic experimental data also shows good correlation of measured effective values and the predicted ones.
(6) The proposed numerical procedure for the estimation of effective elastic properties can be further applied also to other nano- or micro-heterogeneous structural composites in order to assess their anisotropic stiffness matrices or to optimize their composition.

Acknowledgment

Support of the Czech Science Foundation (P105/12/0824 and P105/12/0331) and the Grant Agency of the Czech Technical University in Prague (SGS12/116/OHK1/2T/11) is gratefully acknowledged.

References

[1] Ulm F-J, Vandamme M, Bobko C, Ortega JA. Statistical indentation techniques for hydrated nanocomposites: concrete, bone, and shale. J Am Ceram Soc 2007;90(9):2677–92.
[2] Constantinides G, Chandran KR, Ulm F-J, Vliet KV. Grid indentation analysis of composite microstructure and mechanics: principles and validation. Mater Sci Eng: A 2006;430(1–2):189–202.
[3] Němeček J, Šmilauer V, Kopecký L. Nanoindentation characteristics of alkali-activated aluminosilicate materials. Cem Concr Compos 2011;33(2):163–70.
[4] Sorelli L, Constantinides G, Ulm F-J, Toutlemonde F. The nano-mechanical signature of ultra high performance concrete by statistical nanoindentation techniques. Cem Concr Res 2008;38(12):1447–56.
[5] Fischer-Cripps AC. Nanoindentation. New York: Springer Verlag; 2002.
[6] Zaoui A. Continuum micromechanics: survey. J Eng Mech 2002;128:808–16.
[7] Němeček J. Creep effects in nanoindentation of hydrated phases of cement pastes. Mater Characterization 2009;60(9):1028–34.
[8] Singh NB, Middendorf B. Calcium sulfate hemihydrate hydration leading to gypsum crystallization. Prog Crystal Growth Characterization Mater 2007;53(1):57–77.
[9] Miyoshi T, Itoh M, Akiyama S, Kitahara A. Aluminium foam "ALPORAS": the production process, properties and application. Mater Res Soc Sympos Proc 1998:521.
[10] Němeček J, Králík V, Vondřejc J, Němečková J. Identification of micromechanical properties on metal foams using nanoindentation. In: Proceedings of the thirteenth international conference on civil, structural and environmental engineering computiing [CD-ROM]. Edinburgh: Civil-Comp Press; 2011. p. 1–12 [ISBN 978-1-905088-46-1].
[11] Simone AE, Gibson LJ. Aluminum foams produced by liquid-state processes. Acta Mater 1998;46(9):3109–23.
[12] Oliver WC, Pharr GM. An improved technique for determining hardness and elastic modulus using load and displacement sensing indentation experiments. J Mater Res 1992;7(6):1564–83.
[13] Swadener JG, Pharr GM. Indentation of elastically anisotropic half-spaces by cones and parabolae of revolution. Phil Mag A 2001;81(2):447–66.
[14] Vlassak JJ, Ciavarella M, Barber JR, Wang X. The indentation modulus of elastically anisotropic materials for indenters of arbitrary shape. J Mech Phys Solids 2003;51:1701–21.
[15] Eshelby JD. The determination of the elastic field of an ellipsoidal inclusion and related problems. Proc R Soc London A 1957;241:376–96.
[16] Mori T, Tanaka K. Average stress in the matrix and average elastic energy of materials with misfitting inclusions. Acta Metall 1973;21(5):571–4.
[17] Moulinec H, Suquet P. A fast numerical method for computing the linear and nonlinear mechanical properties of composites. Comptes rendus del'Académie des sciences. Série II, Mécanique, physique, chimie, astronomie 1994; 318(11): 1417–1423.
[18] Moulinec H, Suquet P. A numerical method for computing the overall response of nonlinear composites with complex microstructure. Comput Methods Appl Mech Eng 1998;157(1–2):69–94.
[19] Saranen J, Vainikko G. Periodic integral and pseudodifferential equations with numerical approximation. Berlin: Springer; 2002.
[20] Vainikko G. Fast solvers of the Lippmann–Schwinger equation. In: Gilbert RP, Kajiwara J, Xu YS, editors. Direct and inverse problems of mathematical physics, international society for analysis applications and computation, vol. 5. Dordrecht (The Netherlands): Kluwer Academic Publishers; 2000. p. 423–40.
[21] Zeman J, Vondřejc J, Novák J, Marek I. Accelerating a FFT-based solver for numerical homogenization of periodic media by conjugate gradients. J Comput Phys 2010;229(21):8065–71.
[22] Velez K et al. Determination of nanoindentation of elastic modulus and hardness of pure constituents of Portland cement clinker. Cem Concr Res 2001;31:555–61.
[23] Constantinides G, Ulm F-J. The nanogranular nature of C–S–H. J Mech Phys Solids 2007;55:64–90.
[24] Constantinides G, Ulm F-J. The effect of two types of C–S–H on the elasticity of cement-based materials: results from nanoindentation and micromechanical modeling. Cem Concr Res 2004;34(1):67–80.
[25] Hughes JJ, Trtik P. Micro-mechanical properties of cement paste measured by depth-sensing nanoindentation: a preliminary correlation of physical properties with phase type. Mater Characterization 2004;53:223–31.
[26] Meille S, Garboczi EJ. Linear elastic properties of 2D and 3D models of porous materials made from elongated objects. Modell Simul Mater Sci Eng 2001;9(5):371–90.
[27] Garboczi et al. Modeling and measuring the structure and properties of cement-based materials, National Institute of Standards and Technology; 1989–2011. <http://ciks.cbt.nist.gov/garbocz/monograph>.
[28] Sanahuja J, Dormieux L, Meille S, Hellmich C, Fritsch A. Micromechanical explanation of elasticity and strength of gypsum: from elongated anisotropic crystals to isotropic porous polycrystals. J Eng Mech 2010;136(2):239–53.
[29] Jeon I et al. Cell wall mechanical properties of closed-cell Al foam. Mech Mater 2009;41:60–73.
[30] Ashby MF, Evans AG, Fleck NA, Gibson LJ, Hutchinson JW, Wadley HNG. Metal Foams: A Design Guide. Butterworth-Heinemann; 2000.